Eur. Phys. J. A (2017) **53**: 69
DOI 10.1140/epja/i2017-12258-9

THE EUROPEAN PHYSICAL JOURNAL A

Regular Article – Experimental Physics

# Identification of levels above $6^-$ isomeric state in $^{66}$Cu

Purnima Singh[1,a], R. Palit[1], D. Choudhury[2], P.C. Srivastava[3], S. Biswas[1], S. Saha[1], and J. Sethi[1,4]

[1] Department of Nuclear and Atomic Physics, Tata Institute of Fundamental Research, Mumbai - 400005, India
[2] ELI-NP, Horia Hulubei National Institute for Physics and Nuclear Engineering, 077125 Magurele, Romania
[3] Department of Physics, Indian Institute of Technology Roorkee, Roorkee 247 667, India
[4] Department of Chemistry and Biochemistry, University of Maryland, College Park, MD - 20742, USA

Received: 21 February 2017
Published online: 12 April 2017 – 
Communicated by P. Woods

**Abstract.** Excited states in odd-odd $^{66}$Cu were investigated in a reaction between a 136 MeV $^{30}$Si beam and a $^{65}$Cu target with the Indian National Gamma Array. Six new transitions have been identified including four transitions feeding the 600 ns $6^-$ isomeric state from an investigation of prompt-prompt and prompt-delayed coincidence events. The results of the present work have extended the level structure of this nucleus up to $I^\pi = (9^-)$. In addition, new information on the set of $\pi p_{3/2}\nu g_{9/2}$ multiplets in this nucleus have been added. Shell model calculations were performed within the $fpg_{9/2}$ and $f_{5/2}pg_{9/2}$ model spaces. The results of shell model calculations using the $fpg_{9/2}$ model space have been observed to be in better agreement with experimental excitation energies up to the highest spin observed. The results of the present work highlight the necessity of $f_{7/2}$ proton holes to describe the positive as well as negative parity states in $^{66}$Cu.

## 1 Introduction

In recent years, the structure of neutron-rich nuclei in the vicinity of $^{68}$Ni has been investigated extensively, since they provide significant insight into shell structure evolution away from stability. A subject of extensive debate in these studies has been the behavior of neutron subshell closure at $N = 40$, which separates the $pf$ shell from the intruder $g_{9/2}$ state. The doubly magic character of $^{68}$Ni ($Z = 28$, $N = 40$), has been substantiated by a high excitation energy of the $I^\pi = 2_1^+$ state as well as a very small $B(E2, 2_1^+ \longrightarrow 0^+)$ value [1,2]. The observation of several isomeric states in $^{68}$Ni and neighboring nuclei further corroborate its magic character [3]. On the other hand, the quasi-constant behavior of two-neutron separation energies around $N = 40$ does not support a shell closure [4]. It has been proposed that the semi-magic subshell closure at $N = 40$ is possibly related to the parity change between the $pf$ shell and the $g_{9/2}$ orbital [2,5].

The low-excitation energy of the $2_1^+$ state in $^{66}$Fe [6] and unexpectedly large $B(E2)$ values in $^{70}$Ni [7] has led to the suggestion that adding or removing a few nucleons to $^{68}$Ni leads to the disappearance of the magicity at $N = 40$. The quenching of this subshell gap was attributed to the strong interaction between the $pf$ protons and the $g_{9/2}$ neutrons. Thus, a weakening of the $Z = 28$ and $N = 40$ gaps results, when neutrons start filling the $g_{9/2}$ orbitals in neutron-rich nuclei beyond and below $^{68}$Ni leading to a collective behavior. These suggestions were once again challenged by the observation of a large energy gap above the $19/2^-$ isomeric state in $^{71}$Cu [8], which was interpreted as a support of the stability of the $N = 40$ shell gap.

Besides the fragility of the $N = 40$ stabilization effect and its influence on the structure around $^{68}$Ni, the importance of the proton excitations across the $Z = 28$ shell gap for the correct description of nuclei in this region is also an area of current interest [9,10].

From the discussions above, it is clear that a coherent description of various nuclear structure phenomena in this mass region is still far from being complete. This is also reflected in various ongoing theoretical efforts to determine the most appropriate interaction for use in the shell model calculations [11,12]. The Cu ($Z = 29$) isotopes, having a single proton outside the Ni ($Z = 28$) core, provide an ideal testing ground for these modern effective interactions, owing to the relative simplicity of their proton states. Further, experimental data on these nuclei, especially the odd-odd isotopes, which are more sensitive to the proton-neutron interaction and configuration mixing, will provide a more stringent test to the calculations.

Experimental investigations in heavier odd-odd Cu isotopes $^{68,70,72}$Cu have led to the observation of $\pi p_{3/2}\nu g_{9/2}$-based multiplet structures [13–16]. A systematic study of these states could probe the interaction between $\pi p_{3/2}$ and $\nu g_{9/2}$ orbitals, which are expected to play crucial role in neutron-rich nuclei in $^{78}$Ni region. However,

[a] e-mail: purnima.phy@gmail.com

so far, there is little information known on these structures in lighter odd-odd isotopes $^{64,66}$Cu. Furthermore, in a recent work on the spectroscopic quadrupole moment measurement of the $6^-$ isomeric state in $^{66}$Cu [17], this state was proposed to involve a weak coupling of the $\pi p_{3/2}$ and $\nu g_{9/2}$ orbitals resulting into an oblate shape. It would be of great interest to observe the behavior of the structure built on top of this isomer to further explore the nature of its deformation.

The low-lying excited states of the odd-odd nucleus $^{66}$Cu have been the subject of several experimental investigations in the past (see ref. [18] and references therein). This nucleus has been studied using $\beta$-decay of $^{66}$Ni [19], neutron capture $(n, \gamma)$ [20, 21], stripping and pickup reactions [22–25]. Despite these efforts, many details of the level structure are either unknown or poorly established.

In the present work, six new transitions have been identified including four transitions feeding the $6^-$ isomeric state from an investigation of prompt-delayed coincidence events in a multinucleon transfer reaction. In sect. 2, the experimental setup and the offline data analysis techniques are briefly outlined. The experimental results and level scheme are presented in sect. 3. The experimental results are interpreted in the framework of spherical shell model in sect. 4. Finally, a summary of the present work is given in sect. 5.

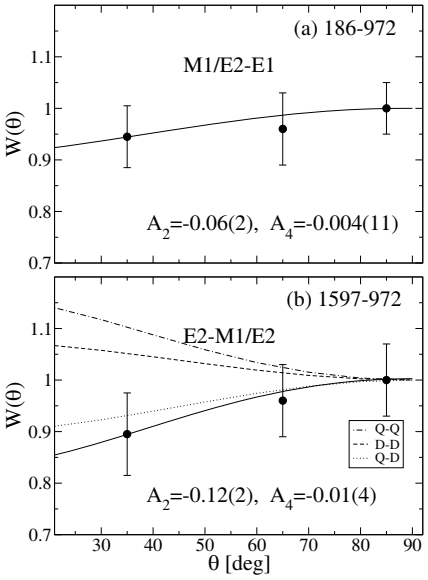


**Fig. 1.** Measured angular correlations (solid circles) for $\gamma\gamma$ cascades in $^{66}$Cu. The best-fit calculated curves for the multipolarities given in the figure are shown as solid lines. The dot, dashed and dot-dashed lines in panel (b) correspond to the expected patterns associated with pairs of stretched quadrupole-dipole, pure stretched dipole-dipole and stretched quadrupole-quadrupole pairs, respectively.

## 2 Experimental details and analysis

Excited states of $^{66}$Cu were populated using multinucleon transfer reaction between a $^{30}$Si beam and a $^{65}$Cu target. The 136 MeV $^{30}$Si beam was provided by the TIFR-BARC Pelletron LINAC facility at Tata Institute of Fundamental Research (TIFR) Mumbai. The target consisted of a 1.0 mg/cm$^2$ thick foil of isotopically enriched $^{65}$Cu rolled with a 13.8 mg/cm$^2$ thick $^{197}$Au foil. The $\gamma$-rays emitted by the reaction products were detected with the Indian National Gamma Array (INGA) spectrometer consisting of 19 Compton-suppressed HPGe clover detectors arranged in six rings at 40°, 65°, 90°, 115°, 140°, and 157° with respect to the beam direction [26]. Two- and higher-fold clover coincidence events were collected in a fast digital data acquisition (DDAQ) system based on Pixie-16 modules of XIA LLC [27]. The $\gamma$-ray energies and efficiencies were calibrated with the standard $^{152}$Eu and $^{133}$Ba radioactive source.

For the offline analysis, the data sorting routine "MultipARameter time-stamped-based COincidence Search program (MARCOS)", was used to sort the time-stamped data and generate one-dimensional histograms, $\gamma^2$ matrices and $\gamma^3$ cubes. The time window for the prompt $\gamma$-$\gamma$ coincidence was set to 200 ns. In order to identify states above the isomeric level, prompt-delayed coincidence analysis technique was used. In this approach, the prompt $\gamma$-ray transitions (within a time window of 100 ns) above the isomer were stored on one axis of the matrix (the prompt axis) and the delayed $\gamma$-ray transitions following the decay of isomer (within a time window 400–800 ns) were stored on the other axis (the delayed axis). Detailed discussion on this technique can be found in ref. [28]. The data analysis was done using the software package RADWARE [29].

To determine the spin of excited states in $^{66}$Cu, an angular correlation analysis of the de-exciting $\gamma$-rays was performed [30]. The pairs of clover detectors were divided into three groups with average angles 35°, 65° and 85° between them. Three two-dimensional coincidence matrices were created, each corresponding to one of the three angle groups. For every pair of prompt $\gamma$-rays with energies $E_{\gamma 1}$, $E_{\gamma 2}$ and relative angle $\theta$, the angular correlation matrix for the corresponding angle group was incremented. Background-subtracted spectra were projected from each of the three angular correlation matrices by gating on one of the transitions in $^{66}$Cu. The fitted peak areas for coincident $\gamma$-rays were corrected for efficiency of the Ge detectors and a normalization for the number of pairs of detectors in the specific angle group. The resulting intensity $W(\theta)$ was least-squares fitted with the standard Legendre-polynomial expression,

$$W(\theta) = A_0[1 + A_2 P_2(\cos\theta) + A_4 P_4(\cos\theta)], \qquad (1)$$

to determine the angular correlation coefficients $A_2$ and $A_4$. These values were then used to determine the multipolarity of the other transition. The method was checked for the present INGA geometry, by analyzing the angular correlations of transitions belonging to standard radioactive sources and yrast cascades of the fission fragments having well-known multipole orders [28]. Figure 1 presents the angular correlation data compared to theoretical curves for the newly assigned multipolarities in $^{66}$Cu (see also sect. 3).

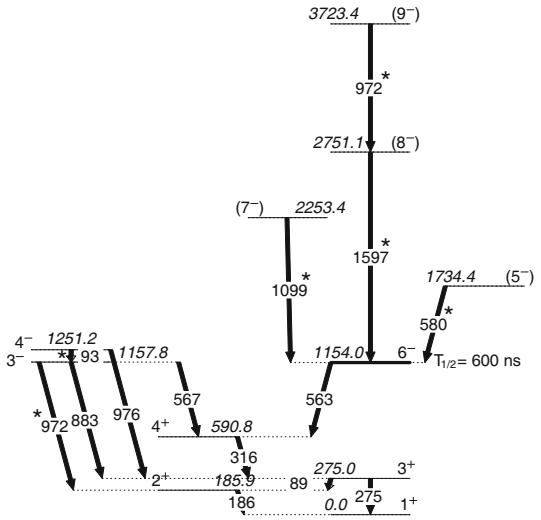


**Fig. 2.** Partial level scheme of $^{66}$Cu. The transitions newly identified in the present work are marked with asterisks.

**Table 1.** List of levels with the spin-parity assignments and $\gamma$-rays identified in $^{66}$Cu. The uncertainties in the energies of the $\gamma$-ray is between 0.5 and 1.0 keV. The intensities for $\gamma$-rays above the $6^-$ isomeric state are normalized to the 1597.1 keV transition, with $I_\gamma = 100$.

| $E_i$ | $J_i^\pi$ | → | $J_f^\pi$ | $E_\gamma$ | $I_\gamma$ |
|---|---|---|---|---|---|
| 185.9 | $2^+$ | → | $1^+$ | 185.9 | |
| 275.0 | $3^+$ | → | $2^+$ | 89.1 | |
| | $3^+$ | → | $1^+$ | 275.0 | |
| 590.8 | $4^+$ | → | $3^+$ | 315.8 | |
| 1154.0 | $6^-$ | → | $4^+$ | 563.2 | |
| 1157.8 | $3^-$ | → | $4^+$ | 567.0 | |
| | $3^-$ | → | $3^+$ | 882.8 | |
| | $3^-$ | → | $2^+$ | 971.9 | |
| 1251.2 | $4^-$ | → | $3^-$ | 93.4 | |
| | $4^-$ | → | $3^+$ | 976.2 | |
| 1734.4 | $(5^-)$ | → | $6^-$ | 580.4 | 85(8) |
| 2253.4 | $(7^-)$ | → | $6^-$ | 1099.4 | 62(7) |
| 2751.1 | $(8^-)$ | → | $6^-$ | 1597.1 | 100 |
| 3723.4 | $(9^-)$ | → | $(8^-)$ | 972.3 | 32(4) |

## 3 Results and level scheme

The level scheme of $^{66}$Cu established from the present work is shown in fig. 2. The transitions have been placed on the basis of prompt-prompt and prompt-delayed $\gamma$-$\gamma$ coincidence relations and relative $\gamma$-transition intensities. Spin and parity assignments to the states have been made on the basis of angular correlation analysis, systematics or adapted from literature values [18]. The experimental information on levels in $^{66}$Cu is summarized in table 1.

Prior to this work, the nucleus $^{66}$Cu was studied using a variety of reactions and decay measurements (ref. [18] and references therein). Representative double-gated coincidence spectrum confirming part of the previously established decay scheme is given in fig. 3(a). The $I^\pi$ assignments for the ground, 186 keV, 275 keV and 591 keV states have already been well established as $1^+$, $2^+$, $3^+$ and $4^+$, respectively, through several experimental techniques (see the summary in ref. [18]). In the following we will discuss the new features of the level scheme.

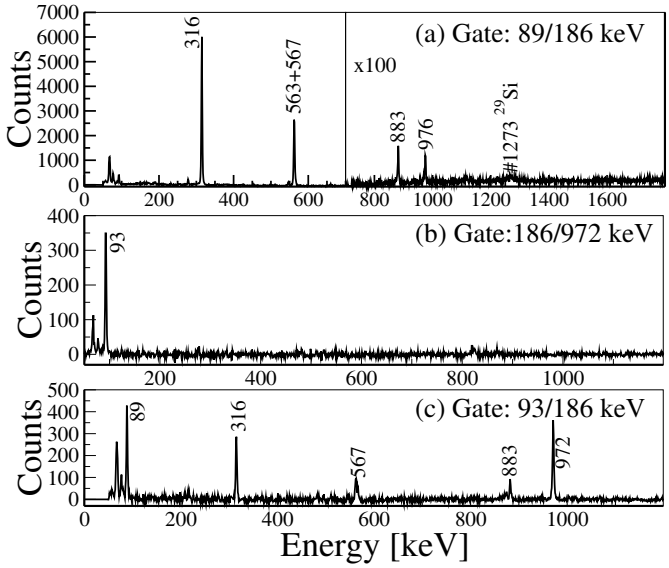


**Fig. 3.** Background-subtracted coincidence spectra double gated in the prompt cube on transitions at (a) 89/186 keV (b) 186/972 keV and (c) 93/186 keV. The 1273 keV line in (a) is a cross-coincidence transition from the complimentary projectile-like reaction partner $^{29}$Si.

The evaluation of ref. [18] lists two unique levels at 1154 and 1158 keV. The 1154 keV state has been studied in detail in various transfer reactions. It was observed to be an isomeric state decaying via an M2 transition to the 591 keV level and has been assigned an $I^\pi = 6^-$ [23]. The 1158 keV level was earlier reported in $(n,\gamma)$ [20] and $(t,{}^3He)$ [24] reactions and was assigned a tentative spin of $(2^+, 3)$ based on its decay to low-lying states. In the present work, we have been able to confirm both these levels. Our present angular correlation analysis suggests E1 nature for the 971.9 keV transition, thus an $I^\pi = 3^-$ has been assigned to the 1158 keV level. A level at 1247 keV was reported in various prior experimental works (see ref. [18] and references therein). The level was assigned an $I^\pi = 4^-$ [23]. A transition of 972.1 keV was reported to be depopulating this level to the level at 275 keV [20]. In the present work, the high resolution of HPGe detectors has enabled us to identify a doublet peak consisting of 971.9 and 976.2 keV transitions. Through coincidence analysis, we have established the 976.2 keV transition to be depopulating the $I^\pi = 4^-$ level and the 971.9 keV transition to be depopulating the $I^\pi = 3^-$. Thus, the excitation energy of 1247 keV level has been changed to 1251 keV. A strong 93.4 keV transition was observed to decay from this level to the $I^\pi = 3^-$ level (fig. 3(b) and (c)).

As mentioned in previous sections, the 1154 keV, $T_{1/2} = 600\ (20)$ ns, isomeric state in $^{66}$Cu was assigned

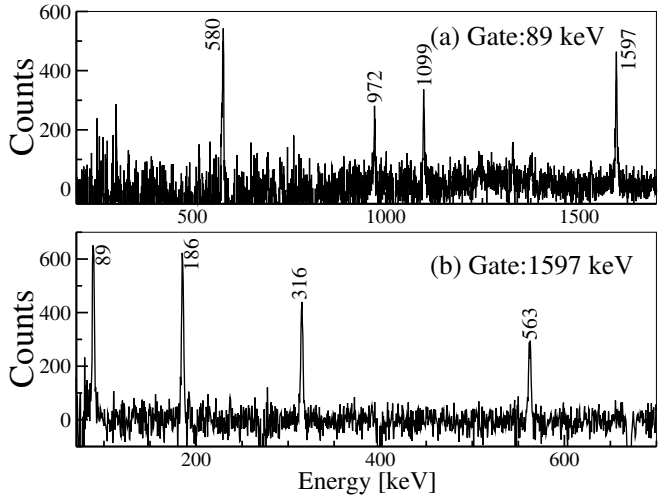


**Fig. 4.** Background-subtracted coincidence spectra gated in the prompt-delayed matrix on transitions at (a) 89 keV and (b) 1597 keV.

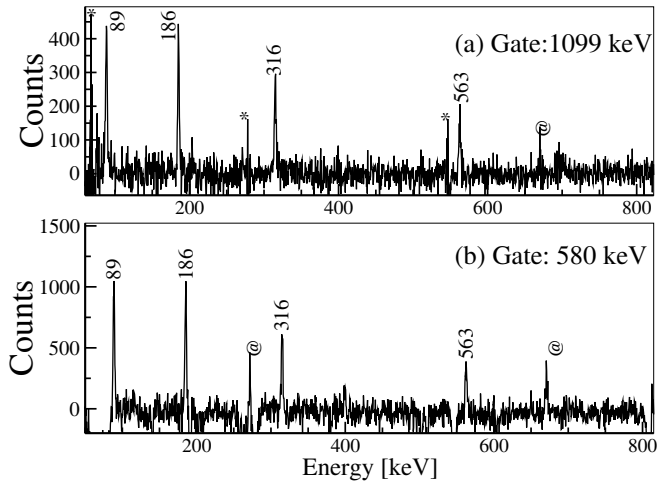


**Fig. 5.** Background-subtracted coincidence spectra gated in the prompt-delayed matrix on transitions at (a) 1099 keV and (b) 580 keV. The peaks marked with * are Coulex from $^{197}$Au backing, @-marked peaks are weak contamination from the nuclei populated in the fusion evaporation reaction $^{65}$Cu($^{30}$Si, $xpxn$).

$I^\pi = 6^-$ in various prior experimental works [18]. To date, no transition above this long-lived state has been reported. In the present work, transitions feeding the isomer were identified by using the prompt-delayed coincidence data. A coincidence spectrum from the prompt-delayed matrix with gate on delayed 89.1 keV transition is shown in fig. 4(a). Four $\gamma$-rays are clearly visible at 580.4, 972.3, 1099.4 and 1597.1 keV. To further confirm these transitions, a prompt gate was applied on 1597.1 keV transition to look for transitions below the $T_{1/2} = 600\ (20)$ ns isomer. As seen in fig. 4(b), 315.8, 89.1, 185.9, and 563.2 keV $\gamma$-rays are clearly visible. Figure 5 supports the feeding of the isomeric state by 1099.4 and 580.4 keV transitions.

In order to establish the mutual coincidence relations between the newly identified transitions, a $\gamma^3$ coincidence

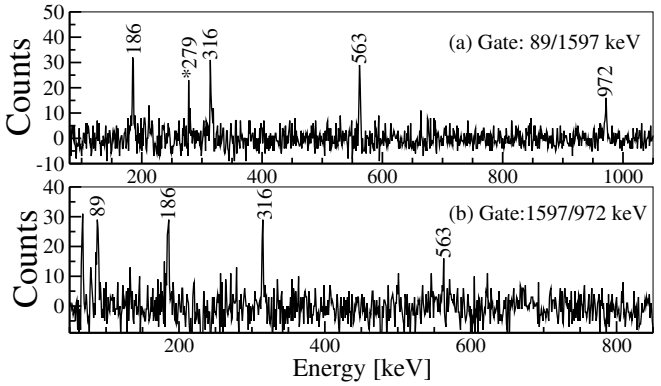


**Fig. 6.** Background-subtracted coincidence spectra double gated in the 1200 ns cube on transitions at (a) 89/1597 keV and (b) 1597/972 keV. The peak marked with * is Coulex from $^{197}$Au backing.

cube was sorted using a coincidence window of 1200 ns. The cube was double gated with one of the newly identified transitions and one previously established transition in $^{66}$Cu. The results, displayed in fig 6(a), establish the feeding of the $^{66}$Cu isomer by the 1597.1–972.3 keV cascade (see fig. 2). This placement was further confirmed by the analysis of the data, where a double gate on the 1597.1 and 972.3 keV $\gamma$-rays yields the spectrum of fig. 6(b), in which the 315.8, 89.1, 185.9, and 563.2 keV $\gamma$-rays are clearly visible. The observed levels above the isomeric state in $^{66}$Cu resemble closely to the positive-parity states in single proton-hole $^{65}$Ni core [31].

The measured angular correlation pattern for the 1597.1–972.3 keV pair favors a sequence with two stretched quadrupole-dipole transitions as can be seen from fig. 1. Due to the similarity of the observed levels to the neighboring nucleus $^{65}$Ni, the 1597.1 keV transition is proposed as a quadrupole transition, leading to a $8^-$ assignment to the level at 2751 and $9^-$ spin assignment for the 3723 keV level. The present statistics was not sufficient to perform angular correlation analysis for the 580.4 or 1099.4 keV transitions, however tentative spin assignments to the levels depopulating these gamma-rays have been made based on systematics.

The observed 1734 keV level in the present work can be correlated with the $\sim$ 1735 keV ($I^\pi = (4,5)^-$) level reported in refs. [24] and [25], which was observed to have large $L = 4(5)$ strength in the $(d,p)$ ($(d,\alpha)$) reactions [25]. The decay pattern of this level bears close similarity to the $I^\pi = 5^-$ level in $^{70}$Cu, where a 511 keV $\gamma$-ray was observed to connect the $I^\pi = 5^-$ state to the $I^\pi = 6^-$ state [14]. Thus, we have proposed a tentative spin of $I^\pi = 5^-$ for the 1734 keV state. Similarly, a spin of $I^\pi = 7^-$ has been proposed for the level at 2253 keV by comparing with the 2186 keV, $I^\pi = 11/2^+$ level in $^{65}$Ni [31].

## 4 Discussion

The structure of even-$A$ Cu isotopes is dominated by the coupling between the odd proton and odd neutron in one

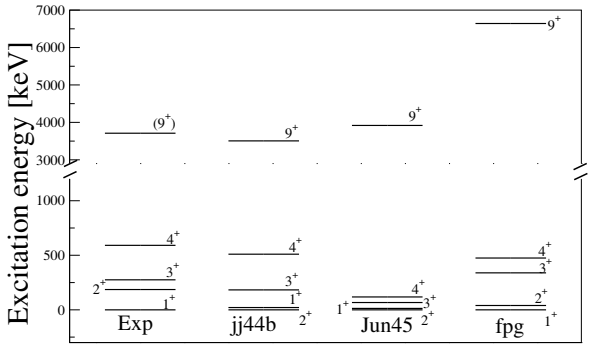


**Fig. 7.** Experimental positive-parity levels in $^{66}$Cu compared to shell model calculations using the jj44b, JUN45, and *fpg* interactions. The experimental data for the $I^\pi = 9^+$ state has been taken from ref. [42].

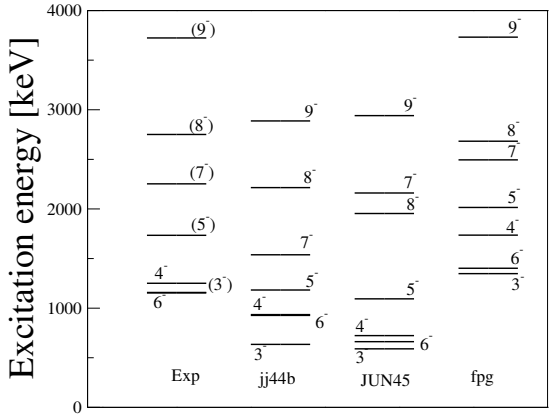


**Fig. 8.** Experimental negative-parity levels in $^{66}$Cu compared to shell model calculations using the jj44b, JUN45, and *fpg* interactions.

of the $p_{3/2}$, $f_{5/2}$, $p_{1/2}$, or $g_{9/2}$ orbitals. In a simple shell model picture, the low-lying level structure of $^{66}$Cu can be regarded as one $p_{3/2}$ proton coupled to one neutron in $f_{5/2}$ orbital. Higher lying states should involve neutron excitations to $p_{1/2}g_{9/2}$ orbitals and proton excitations across $Z = 28$ shell closure.

In order to gain detailed insight into the nature of the observed $^{66}$Cu states, large-scale shell model calculations were carried out using two different model spaces. First set of calculations were performed in the $f_{5/2}pg_{9/2}$ model space using the shell model code NuShellX@MSU [32]. The valence space employed in the calculations comprises the major shell from $Z, N = 28$–$50$, with an inert $^{56}$Ni core. The valence particles were allowed to move freely between the $f_{5/2}$, $p_{3/2}$, $p_{1/2}$, and $g_{9/2}$ orbitals. Two recently derived effective interactions, JUN45 [11] and jj44b [33] have been used in the calculations. Shell model calculations using both these effective interactions have been extensively used to describe the level structure of neighboring nuclei [10,34,35]. The single-particle energies used with the JUN45 interaction are $-8.7087$ ($f_{5/2}$), $-9.8280$ ($p_{3/2}$), $-7.8388$ ($p_{1/2}$), and $-6.2617$ ($g_{9/2}$) MeV. These values have been derived by fitting the experimental binding and excitation energies of 69 nuclei in the region $A = 63$–$96$ with $Z \sim 32$ and $N \sim 50$ [11]. The fitting for JUN45 interaction excludes explicitly the Ni and Cu isotopes since the $^{56}$Ni core is viewed as being soft. For the jj44b interaction, the single particle energies are $-9.6566$ ($p_{3/2}$), $-9.2859$ ($f_{5/2}$), $-8.2695$ ($p_{1/2}$), and $-5.8944$ ($g_{9/2}$) MeV. In jj44b interaction, experimental data from $Z = 28$–$30$ isotopes and $N = 48$–$50$ isotones were included in the fits.

To explore the role of proton excitation across $Z = 28$ shell closure, we have also performed a second set of calculations with $fpg_{9/2}$ model space using shell model code Antoine [36]. In this valence space, we use a $^{48}$Ca core (with eight neutrons frozen in the $\nu f_{7/2}$ orbital). The *fpg* interaction used in present calculations was originally reported by Sorlin *et al.* [37] and further modification of 28 two-body matrix elements of the earlier interaction have been done in ref. [38] by changing $\pi f_{5/2}\nu g_{9/2}$ and $\pi f_{7/2}\nu g_{9/2}$ matrix elements to get better spectroscopic properties in this region. The original *fpg* interaction for $fpg_{9/2}$ valence space was developed using *fp* two-body matrix elements (TBME) from ref. [39] and *rg* TBME ($p_{3/2}$, $f_{5/2}$, $p_{1/2}$ and $g_{9/2}$ orbitals) from ref. [40]. For the common active orbitals in these subspaces, matrix elements were taken from ref. [40]. The remaining $f_{7/2}g_{9/2}$ TBME are taken from ref. [41]. The single-particle energies are 0.0 ($f_{7/2}$), 2.0 ($p_{3/2}$), 4.0 ($p_{1/2}$), 6.5 ($f_{5/2}$), and 9.0 ($g_{9/2}$) MeV. For this model space we allowed two particle excitations from the $f_{7/2}$ orbital to the upper *fp* orbitals for protons and from the upper *fp* orbitals to the $g_{9/2}$ orbital for neutrons.

A comparison of the experimental excitation energies of the positive and negative parity states of $^{66}$Cu with the predictions of shell model calculations are shown in figs. 7 and 8, respectively. For clarity, only the calculated yrast excitations are shown in the figures. The dominant wave functions are shown in table 2.

Both the $f_{5/2}pg_{9/2}$ interactions fail to reproduce the ground state $1^+$ of $^{66}$Cu. Similar discrepancies were reported in other odd-odd Cu isotopes by Vingerhoets *et al.* [35]. A highly mixed ground state with a dominant contribution from $\pi(p^1_{3/2}) \otimes \nu(p^4_{3/2}f^4_{5/2}p^1_{1/2}g^0_{9/2})$ configuration is predicted by both the interactions. The *fpg* interaction correctly reproduces the ground state and predicts a dominant $\pi(p^1_{3/2}) \otimes \nu(p^4_{3/2}f^3_{5/2}p^2_{1/2}g^0_{9/2})$ ($\sim$ 42%) configuration and $\sim$ 20% contribution from $\pi(p^1_{3/2}) \otimes \nu(p^4_{3/2}f^4_{5/2}p^1_{1/2}g^0_{9/2})$ configuration. A significant $\nu p_{1/2}$ occupation is also supported by a recent *g*-factor measurement using the technique of collinear laser spectroscopy [35]. The positive parity levels calculated using the *fpg* interaction lie within 150 keV of experiment. The calculations also predict about 15–20% contribution of configurations involving excitations from the $\pi f_{7/2}$ orbital in the wave function of positive parity states. In general, jj44b shows better agreement with experiment than JUN45, which could be due to the fact that this interaction was obtained by fits including Ni and Cu isotopes whose structure are known to be influenced by the $\pi f_{7/2}$ orbitals. The JUN45 spectrum is too compressed, with calculations

**Table 2.** Dominant partitions of wave functions of the positive and negative parity states in $^{66}$Cu.

| jj44b | | | | |
|---|---|---|---|---|
| | | Wave functions | | |
| $I$ | Excitation energy (keV) | Probability | Proton | Neutron |
| $1^+$ | 21 | 30.8% | $p^1_{3/2}$ | $p^4_{3/2}f^4_{5/2}p^1_{1/2}g^0_{9/2}$ |
| $2^+$ | 0 | 33.3% | $p^1_{3/2}$ | $p^4_{3/2}f^4_{5/2}p^1_{1/2}g^0_{9/2}$ |
| $3^+$ | 183 | 20.3% | $p^1_{3/2}$ | $p^4_{3/2}f^3_{5/2}p^2_{1/2}g^0_{9/2}$ |
| $4^+$ | 510 | 25.8% | $p^1_{3/2}$ | $p^4_{3/2}f^3_{5/2}p^2_{1/2}g^0_{9/2}$ |
| $9^+$ | 3506 | 13.7% | $g^1_{9/2}$ | $p^4_{3/2}f^4_{5/2}p^0_{1/2}g^1_{9/2}$ |
| $3^-$ | 635 | 22.0% | $p^1_{3/2}$ | $p^4_{3/2}f^4_{5/2}p^0_{1/2}g^1_{9/2}$ |
| $4^-$ | 927 | 17.6% | $p^1_{3/2}$ | $p^4_{3/2}f^4_{5/2}p^0_{1/2}g^1_{9/2}$ |
| $5^-$ | 1183 | 15.4% | $p^1_{3/2}$ | $p^4_{3/2}f^4_{5/2}p^0_{1/2}g^1_{9/2}$ |
| $6^-$ | 935 | 23.1% | $p^1_{3/2}$ | $p^4_{3/2}f^4_{5/2}p^0_{1/2}g^1_{9/2}$ |
| $7^-$ | 1538 | 26.9% | $f^1_{5/2}$ | $p^4_{3/2}f^4_{5/2}p^0_{1/2}g^1_{9/2}$ |
| $8^-$ | 2215 | 27.0% | $p^1_{3/2}$ | $p^4_{3/2}f^3_{5/2}p^1_{1/2}g^1_{9/2}$ |
| $9^-$ | 2887 | 31.0% | $f^1_{5/2}$ | $p^4_{3/2}f^4_{5/2}p^0_{1/2}g^1_{9/2}$ |
| JUN45 | | | | |
| | | Wave functions | | |
| $I$ | Excitation energy (keV) | Probability | Proton | Neutron |
| $1^+$ | 67 | 46.5% | $p^1_{3/2}$ | $p^4_{3/2}f^4_{5/2}p^1_{1/2}g^0_{9/2}$ |
| $2^+$ | 0 | 17.8% | $p^1_{3/2}$ | $p^4_{3/2}f^4_{5/2}p^1_{1/2}g^0_{9/2}$ |
| $3^+$ | 13 | 31.2% | $p^1_{3/2}$ | $p^4_{3/2}f^5_{5/2}p^0_{1/2}g^0_{9/2}$ |
| $4^+$ | 118 | 24.2% | $p^1_{3/2}$ | $p^4_{3/2}f^5_{5/2}p^0_{1/2}g^0_{9/2}$ |
| $9^+$ | 3918 | 17.5% | $p^1_{3/2}$ | $p^4_{3/2}f^3_{5/2}p^0_{1/2}g^2_{9/2}$ |
| $3^-$ | 590 | 32.3% | $p^1_{3/2}$ | $p^4_{3/2}f^4_{5/2}p^0_{1/2}g^1_{9/2}$ |
| $4^-$ | 723 | 26.9% | $p^1_{3/2}$ | $p^4_{3/2}f^4_{5/2}p^0_{1/2}g^1_{9/2}$ |
| $5^-$ | 1094 | 29.3% | $p^1_{3/2}$ | $p^4_{3/2}f^4_{5/2}p^0_{1/2}g^1_{9/2}$ |
| $6^-$ | 662 | 32.2% | $p^1_{3/2}$ | $p^4_{3/2}f^4_{5/2}p^0_{1/2}g^1_{9/2}$ |
| $7^-$ | 2161 | 20.8% | $p^1_{3/2}$ | $p^4_{3/2}f^3_{5/2}p^1_{1/2}g^1_{9/2}$ |
| $8^-$ | 1954 | 23.9% | $p^1_{3/2}$ | $p^4_{3/2}f^4_{5/2}p^0_{1/2}g^1_{9/2}$ |
| $9^-$ | 2941 | 27.9% | $p^1_{3/2}$ | $p^4_{3/2}f^4_{5/2}p^0_{1/2}g^1_{9/2}$ |
| *fpg* | | | | |
| | | Wave functions | | |
| $I$ | Excitation energy (keV) | Probability | Proton | Neutron |
| $1^+$ | 0 | 41.8% | $f^8_{7/2}p^1_{3/2}$ | $f^8_{7/2}p^4_{3/2}f^3_{5/2}p^2_{1/2}g^0_{9/2}$ |
| $2^+$ | 40 | 33.0% | $f^8_{7/2}p^1_{3/2}$ | $f^8_{7/2}p^4_{3/2}f^3_{5/2}p^2_{1/2}g^0_{9/2}$ |
| $3^+$ | 339 | 49.2% | $f^8_{7/2}p^1_{3/2}$ | $f^8_{7/2}p^4_{3/2}f^3_{5/2}p^2_{1/2}g^0_{9/2}$ |
| $4^+$ | 475 | 60.0% | $f^8_{7/2}p^1_{3/2}$ | $f^8_{7/2}p^4_{3/2}f^3_{5/2}p^2_{1/2}g^0_{9/2}$ |
| $9^+$ | 6642 | 15.9% | $f^8_{7/2}p^1_{3/2}$ | $f^8_{7/2}p^4_{3/2}f^3_{5/2}p^0_{1/2}g^2_{9/2}$ |
| $3^-$ | 1348 | 29.2% | $f^8_{7/2}p^1_{3/2}$ | $f^8_{7/2}p^4_{3/2}f^2_{5/2}p^2_{1/2}g^1_{9/2}$ |
| $4^-$ | 1736 | 19.7% | $f^8_{7/2}p^1_{3/2}$ | $f^8_{7/2}p^4_{3/2}f^2_{5/2}p^2_{1/2}g^1_{9/2}$ |
| $5^-$ | 2015 | 10.3% | $f^8_{7/2}p^1_{3/2}$ | $f^8_{7/2}p^4_{3/2}f^2_{5/2}p^2_{1/2}g^1_{9/2}$ |
| $6^-$ | 1402 | 28.8% | $f^8_{7/2}p^1_{3/2}$ | $f^8_{7/2}p^4_{3/2}f^2_{5/2}p^2_{1/2}g^1_{9/2}$ |
| $7^-$ | 2495 | 23.9% | $f^8_{7/2}p^1_{3/2}$ | $f^8_{7/2}p^4_{3/2}f^3_{5/2}p^1_{1/2}g^1_{9/2}$ |
| $8^-$ | 2683 | 25.4% | $f^8_{7/2}p^1_{3/2}$ | $f^8_{7/2}p^4_{3/2}f^3_{5/2}p^1_{1/2}g^1_{9/2}$ |
| $9^-$ | 3732 | 29.4% | $f^8_{7/2}p^1_{3/2}$ | $f^8_{7/2}p^3_{3/2}f^3_{5/2}p^2_{1/2}g^1_{9/2}$ |

deviating from experiment as high as 472 keV for the $4^+$ state.

The 3710 keV excitation energy of $I^\pi = 9^+$ state [42] is fairly reproduced by both the $f_{5/2}pg_{9/2}$ interactions within $\sim 200$ keV. The jj44b interaction predicts this state at 3506 keV with a dominant contribution of $\pi(g^1_{9/2}) \otimes \nu(p^4_{3/2}f^4_{5/2}p^0_{1/2}g^1_{9/2})$ configuration. The JUN45 interaction predicts this state at 3918 keV. However, the state is predicted to have a dominant contribution of $\pi(p^1_{3/2}) \otimes \nu(p^4_{3/2}f^3_{5/2}p^0_{1/2}g^2_{9/2})$ configuration and a very small contribution of $\pi(g^1_{9/2}) \otimes \nu(p^4_{3/2}f^4_{5/2}p^0_{1/2}g^1_{9/2})$ (8%) configuration. The *fpg* interaction predicts this state at 6.642 MeV. This discrepancy could be understood from the fact that the truncation scheme in present calculations does not allow excitations to $\pi g_{9/2}$ orbital which is expected to play a crucial role in the formation of this state.

The excitation of a neutron to $g_{9/2}$ orbital is expected to give rise to a multiplet of states, $I^\pi = (3, 4, 5, 6)^-$. Prior to this study, the experimental information on the members of the $\pi p_{3/2}\nu g_{9/2}$ negative parity multiplets in $^{66}$Cu was rather incomplete. Candidates for these states were suggested at 1154 [18], 1734 and 1247 keV [24]. The newly established $I^\pi = 3^-$ for the state at 1158 keV in the present work adds to this set of $\pi p_{3/2}\nu g_{9/2}$ multiplets in $^{66}$Cu. Figure 8 presents a comparison of the negative parity levels in $^{66}$Cu with the shell model calculations using the jj44b, JUN45 and *fpg* interactions. With both JUN45 and jj44b interactions, the energy of the $6^-$ state is predicted lower than the measured value. It is worth noting that the jj44b interaction calculates this state to lie within 219 keV of the data, while the level is predicted to lie 492 keV lower than experiment with JUN45. This is possibly the result of the location of the $\nu g_{9/2}$ orbital at a lower energy in the JUN45 Hamiltonian, as compared to that in jj44b. Both the interactions predict about 20% admixture of the $\nu g^3_{9/2}$ configuration into the $6^-$ wave function, further supporting a low single particle energy of $\nu g_{9/2}$ orbital. The jj44b interaction predicts unusually low-lying $3^-$ and $5^-$ states. A possible reason for this could be the fact that the absence of $\pi f_{7/2}$ orbital from the model space has been taken into account by incorporating its influence into the interactions involving the active $f_{5/2}$, $p_{3/2}$, $p_{1/2}$, and $g_{9/2}$ orbitals. Consequently, the calculations using these compensating interactions are expected to give a poor agreement with experiment for states where $\pi f_{7/2}$ orbital is not involved. Both these states are predicted to have a large admixture of $\pi f^1_{5/2}$ configuration, which is about 13% for $3^-$ and 20% for $5^-$ state. The wave function for all the negative parity states is predicted to be predominantly $\pi(p^1_{3/2}) \otimes \nu(p^4_{3/2}f^4_{5/2}p^0_{1/2}g^1_{9/2})$ for both the interactions. With *fpg* interaction, all the calculated excitation energies are $\sim 250$ keV higher than experiment, which could be attributed to the truncation of the model space due to computational difficulties. However, the results are in general better agreement with experiment as compared to jj44b and JUN45. For these

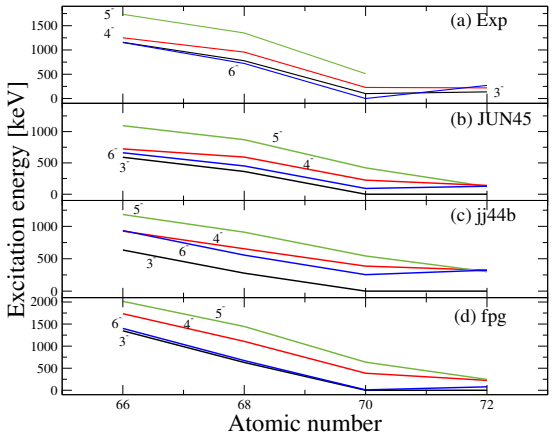


**Fig. 9.** (Color online) (a) Experimental excitation energies of $\pi p_{3/2}\nu g_{9/2}$-based multiplets in $^{66-72}$Cu compared to shell model calculations using (b) JUN45 (c) jj44b and (d) *fpg* interactions.

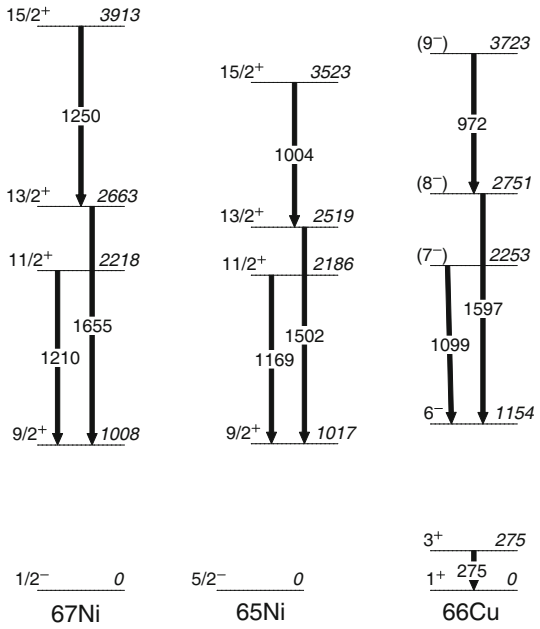


**Fig. 10.** $\nu g_{9/2}$-based structure in $^{66}$Cu compared to the corresponding bands in odd-$A$ Ni isotopes, $^{65}$Ni [31] and $^{67}$Ni [34].

states the dominant contribution predicted by *fpg* interaction is $\pi(p^1_{3/2}) \otimes \nu(p^4_{3/2}f^2_{5/2}p^2_{1/2}g^1_{9/2})$.

The experimental excitation energies of $\pi p_{3/2}\nu g_{9/2}$-based multiplets in $^{66-72}$Cu are compared to the results of shell model calculations in fig. 9. The lowering of these states with increasing neutron number can be attributed to the attractive monopole interaction between the $\pi p_{3/2}$ and $\nu g_{9/2}$ orbitals [11]. The present shell model calculations reasonably describe this feature. However, none of the interactions correctly reproduce the relative splitting and predict the $J = |J_\pi - J_\nu| = 3$ state to be the lowest, whereas in experiment the $J = |J_\pi + J_\nu| = 6$ state appears as the lowest member of this multiplet. This feature of $\pi p_{3/2}\nu g_{9/2}$-based multiplets was already noted by Honma *et al.* [11] in $^{86}$Rb and $^{84}$Br; the authors stressed on the need for an explicit fine-tuning in the $T = 0$ multipole part of the two-body matrix elements for these interactions. It is expected that owing to the relatively simple proton configurations, the current data combined with the available data on odd-odd Cu isotopes could be helpful in tuning these two-body matrix elements for a better description of nuclei in this region. With a difference of 50 keV between the $3^-$ and $6^-$ state, the *fpg* interaction reproduces the splitting better than the other two interactions.

The level structure on top of the $6^-$ isomer in $^{66}$Cu exhibits single-particle character and does not show any evidence for collective behavior. The yrast sequence does not exhibit any regularity in the level spacings that increase with angular momentum, as would be expected in the presence of collectivity. Moreover, the sequence of levels exhibit similarities with the $\nu g_{9/2}$-based structure found above the $9/2^+$ long-lived state in $^{65}$Ni [31] and $^{67}$Ni [34] (see fig. 10). These structures were interpreted in terms of single-particle excitations. By comparison, the level structure in $^{66}$Cu can be understood as a $p_{3/2}$ proton coupled to the $^{65}$Ni core.

The negative parity levels are calculated lower in energy by approximately 700 keV as compared to experiment in jj44b interaction (see fig 8). However, the ordering of levels has a qualitative agreement with experiment. All the negative parity states show a dominant contribution of $\pi p_{3/2}$ orbital except for the $7^-$ and $9^-$ states which predict a dominant contribution from $\pi f_{5/2}$. With the JUN45 interaction, the calculated levels are lower in energy by approximately 800 keV as compared to experiment except for the $7^-$ state. The wave function of $7^-$ state involves about 19% contribution from $\pi f_{5/2}$ orbital, whereas all other states are predicted to involve roughly 80–90% of $\pi p_{3/2}$. A possible reason for this state to be calculated too high in energy in JUN45 interaction could be the lack of inclusion of $Z = 28$ excitations, and this state may involve some contribution from $\pi f_{7/2}$ orbital. The wave function of all other negative-parity states in JUN45 is characterized by a 25–30% component from the $\pi(p^1_{3/2}) \otimes \nu(p^4_{3/2}f^4_{5/2}p^0_{1/2}g^1_{9/2})$ configuration.

As shown in fig. 8, calculations performed using *fpg* interaction are in considerably better agreement with the measured excitation energies, which improves toward higher spin with the calculated level within 10 keV of experiment for $I^\pi = 9^-$ level. The dominant contribution predicted by these calculations is $\pi(p^1_{3/2}) \otimes \nu(p^4_{3/2}f^3_{5/2}p^1_{1/2}g^1_{9/2})$ for $7^-$ and $8^-$ states. The $9^-$ state is predicted to involve a dominant contribution from $\pi(p^1_{3/2}) \otimes \nu(p^3_{3/2}f^3_{5/2}p^2_{1/2}g^1_{9/2})$ ($\sim 29.4\%$) with a significant admixture (22%) from $\pi(p^1_{3/2}) \otimes \nu(p^4_{3/2}f^3_{5/2}p^1_{1/2}g^1_{9/2})$. Furthermore, a significant contribution (15–20%) of configuration involving one or more holes in $\pi f_{7/2}$ orbital is also predicted in all these states.

*Summary of the shell model calculations*: In general, the results of the shell model calculations using the *fpg* interaction have been observed to be in better agreement with the experimental excitation energies up to the highest

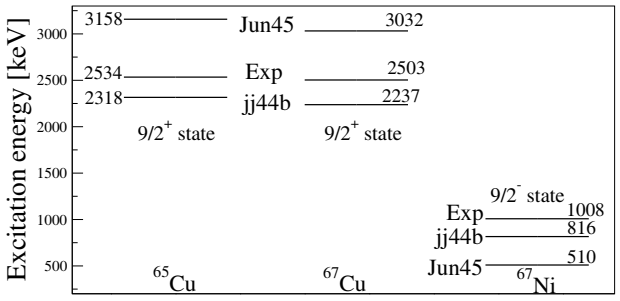


**Fig. 11.** Experimental levels in $^{65,67}$Cu [10], and $^{67}$Ni [34] compared to shell model calculations using the jj44b and JUN45 interactions.

spin observed. The $1^+$ ground state is successfully reproduced and the observed highest spin state $(9^-)$ is reproduced in the calculation within a 10 keV difference. On the other hand, calculations using jj44b and JUN45 show limited success in reproducing experimental data. The overall agreement of the experimental level energies, with those predicted by shell model calculations performed within $fpg_{9/2}$ model space, suggests that the excitations across the $Z = 28$ shell gap play a significant role in forming the positive as well as negative parity yrast structure of this nucleus. A detailed study of electromagnetic transition probabilities can give further insight into the exact nature of wave functions of these states.

It is also desirable to understand the reason for discrepancy between experiment and shell model predictions using JUN45 and jj44b, since both these interactions have been very successful in description of various nuclei in $N, Z = 28$–$50$ region. Figure 11 compares the experimental and calculated excitation energies of $9/2^+$ state in $^{65,67}$Cu ($Z = 29$, $N = 66, 68$). This state involves a dominant contribution from $\pi g_{9/2}$ orbital as suggested by the large $g_{9/2}$ spectroscopic strength deduced in $(^3\mathrm{He}, \mathrm{d})$ transfer studies of $^{65}$Cu [43]. While jj44b predicts this state to lie 200 keV lower than experiment, JUN45 predicts a state 500 keV higher in energy in both the nuclei. In $^{67}$Ni, jj44b predicts the $\nu g_{9/2}$-based $9/2^+$ state to lie 200 keV lower, whereas JUN45 predicts this state to lie 500 keV lower. Similar results were observed in the present work as well. These observations suggest that the adopted single-particle energy of $\nu g_{9/2}$ orbital is lower and $\pi g_{9/2}$ orbital is higher in JUN45. Both the $\nu g_{9/2}$ and $\pi g_{9/2}$ single-particle energies are lower in jj44b. This probably leads to large configuration mixing of the $\nu g_{9/2}$ orbital in the wave function of various states and a poor agreement with experiment as already seen in previous sections on discussion of $^{66}$Cu. However, states with configurations involving both $\nu g_{9/2}$ and $\pi g_{9/2}$ orbitals, such as the $I^\pi = 9^+$ state in $^{66}$Cu, show better agreement with experiment, especially with JUN45 interaction, due to the compensating effect of high and low single-particle energies. Thus, a further optimization of single-particle energies, especially for $g_{9/2}$ orbitals is required for both the interactions to provide a satisfactory description of nuclear structure phenomena in this mass region. In the future, it would also be desirable to perform calculations using the full $fpg_{9/2}$ valence space without any truncation.

## 5 Summary

The level scheme of $^{66}$Cu has been extended up to $I^\pi = 9^-$ using multinucleon transfer reaction with the INGA spectrometer. The results of the present work have added new information on the set of $\pi p_{3/2}\nu g_{9/2}$ multiplets in this nucleus. Energy centroid of a previously observed level has been corrected using the high-resolving power of the spectrometer. In addition, levels above the known 600 ns isomer were established by exploring the prompt and delayed coincidence relationships. Spin and parity for the newly observed states were deduced from angular correlation analysis and comparison with systematics.

Shell model calculations have been carried out with two different model spaces. First set of calculations were carried out in $f_{5/2}pg_{9/2}$ model space using JUN45 and jj44b interactions. The second set of calculations were carried out in $fpg_{9/2}$ model space using $fpg$ interaction. The results of shell model calculations using the $fpg$ interaction have been observed to be in considerably better agreement with experimental excitation energies up to the highest spin observed. These results demonstrate the importance of $f_{7/2}$ proton holes in the description of the positive as well as negative parity states in $^{66}$Cu.

Although the level structure on top of the $6^-$ isomer in $^{66}$Cu exhibits single-particle character and no evidence for any collective behavior was observed, a detailed inspection of calculated wave functions indicates a fairly complex structure for all the states. Calculations indicate a large fragmentation of the amplitudes and contributions by any specific configuration were never found to exceed 50%. Further experimental work aimed at measurement of transition probabilities will be helpful in providing detailed insight into this.

Authors are thankful to the staff at TIFR-BARC Pelletron Linac Facility and all the members of the INGA Collaboration. This work has been partially funded by the Department of Science and Technology, Government of India (No. IR/S2/PF-03/2003-II). Technical support from S. Jadhav, R. Donthi, B.S. Naidu and P.B. Chavan during the experiment is gratefully acknowledged.

## References

1. R. Broda *et al.*, Phys. Rev. Lett. **74**, 868 (1995).
2. O. Sorlin *et al.*, Phys. Rev. Lett. **88**, 092501 (2002).
3. R. Grzywacz *et al.*, Phys. Rev. Lett. **81**, 766 (1998).
4. C. Gunaut *et al.*, Phys. Rev. C **75**, 044303 (2007).
5. H. Grawe *et al.*, Nucl. Phys. A **704**, 211 (2002).
6. M. Hannawald *et al.*, Phys. Rev. Lett. **82**, 1391 (1999).
7. O. Perru *et al.*, Phys. Rev. Lett. **96**, 232501 (2006).
8. I. Stefanescu *et al.*, Phys. Rev. C **79**, 034319 (2009).
9. N.J. Stone *et al.*, Phys. Rev. C **77**, 014315 (2008).

10. C.J. Chiara *et al.*, Phys. Rev. C **85**, 024309 (2012).
11. M. Honma, T. Otsuka, T. Mizusaki, M. Hjorth-Jensen, Phys. Rev. C **80**, 064323 (2009).
12. K. Kaneko, T. Mizusaki, Y. Sun, S. Tazaki, Phys. Rev. C **89**, 011302(R) (2014).
13. I. Stefanescu *et al.*, Phys. Rev. Lett. **98**, 122701 (2007).
14. E. Rapisarda *et al.*, Phys. Rev. C **84**, 064323 (2011).
15. K.T. Flanagan *et al.*, Phys. Rev. **82**, 041302(R) (2010).
16. J.-C. Thomas *et al.*, Phys. Rev. C **74**, 054309 (2006).
17. R.L. Lozeva *et al.*, Phys. Lett. B **694**, 316 (2011).
18. E. Browne, J.K. Tuli, Nucl. Data Sheets **111**, 1093 (2010).
19. N.R. Johnson, R.K. Sheline, R. Wolfgang, Phys. Rev. **102**, 831 (1956).
20. M.G. Delfini, J. Kopecky, R.E. Chrien, H.I. Liou, P.M. Endt, Nucl. Phys. A **404**, 250 (1983).
21. E.B. Shera, H.H. Bolotin, Phys. Rev. **169**, 940 (1968).
22. J.A. Cameron, V.P. Janzen, R.B. Schubank, E.E. Habib, Nucl. Phys. A **425**, 433 (1984).
23. C.L. Woods, J.A. Kuehner, A.A. Pilt, A.J. Trudel, M.C. Vetterli, Nucl. Phys. A **402**, 31 (1983).
24. J.D. Sherman, E.R. Flynn, O. Hansen, N. Stein, J.W. Sunier, Phys. Lett. B **67**, 275 (1977).
25. W.W. Daehnick, Y.S. Park, Phys. Rev. **180**, 1062 (1969).
26. R. Palit *et al.*, Nucl. Instrum. Methods A **680**, 90 (2012).
27. H. Tan *et al.*, in *Proceedings of the IEEE Nuclear Science Symposium Conference Record NSS 08* (IEEE, Washington, DC, 2008) p. 3196.
28. R. Palit, S. Biswas, Pramana **85**, 395 (2015).
29. D.C. Radford, Nucl. Instrum. Methods A **361**, 297 (1995).
30. L.C. Biedenharn, M.E. Rose, Rev. Mod. Phys. **25**, 729 (1953).
31. T. Pawlat, R. Broda, W. Krolas, A. Maj, M. Zieblinski, H. Grawe, R. Schubart, K.H. Maier, J. Heese, H. Kluge, M. Chramm, Nucl. Phys. A **574**, 623 (1994).
32. B.A. Brown, W.D.M. Rae, Nucl. Data Sheets **120**, 115 (2014).
33. B.A. Brown, A.F. Lisetskiy (unpublished), also see endnote [28] in B. Cheal *et al.*, Phys. Rev. Lett. **104**, 252502 (2010).
34. S. Zhu *et al.*, Phys. Rev. C **85**, 034336 (2012).
35. P. Vingerhoets *et al.*, Phys. Rev. C **82**, 064311 (2010).
36. E. Caurier, G. Martínez-Pinedo, F. Nowacki *et al.*, Rev. Mod. Phys. **77**, 427 (2005).
37. O. Sorlin *et al.*, Phys. Rev. Lett. **88**, 092501 (2002).
38. P.C. Srivastava, Mod. Phys. Lett. A **27**, 1250061 (2012).
39. A. Poves, J. Sanchez-Solano, E. Caurier, F. Nowacki, Nucl. Phys. A **694**, 157 (2001).
40. F. Nowacki, Ph.D. Thesis (IRes, Strasbourg, 1996).
41. S. Kahana, H.C. Lee, C.K. Scott, Phys. Rev. **180**, 956 (1969).
42. U. Fister, R. Jahn, P. von Neumann-Cosel, P. Schenk, T.K. Trelle, D. Wenzel, U. Wienands, Nucl. Phys. A **569**, 421 (1994).
43. R.M. Britton, D.L. Watson, Nucl. Phys. A **272**, 91 (1976).